



JOURNAL OF
MARINE
SYSTEMS

www.elsevier.com/locate/jmarsys

CAPÍTOL 4

COMPOSITION AND SPATIO-TEMPORAL VARIABILITY OF PARTICLE FLUXES IN THE WESTERN ALBORAN GYRE, MEDITERRANEAN SEA

J. Fabres¹, A. Calafat¹, A. Sanchez-Vidal¹, M. Canals¹ and S. Heussner²

¹*GRC Geociències Marines, Dept. de Estratigrafia, Paleontologia i Geociències Marines, Universitat de Barcelona, E-08028, Barcelona, Spain*

²*Centre de Formation et Recherche sur l'Environnement Marin, CNRS - UMR 5110, Université de Perpignan, F-66860, Perpignan, France*

* Corresponding author: Tel +34-934021360; Fax +34-934021340.
E-mail address: tonim@natura.geo.ub.es (A. Calafat)

Journal of Marine Systems 33- 34, 431– 456 (2002)

Received 12 January 2001; Accepted 1 June 2001

© Elsevier Science B.V. All rights reserved.

0924-7963/02/\$

doi:10.1016/S0924-7963(02)00070-2

ABSTRACT

Total mass and main constituents (carbonate, organic matter, biogenic opal and lithogenic fraction) flux series were obtained in the northern part of the Western Alboran Gyre during an annual cycle from July 97 to May 98, at 10 days sampling interval. Two mooring lines equipped with sediment trap - current meter pairs were deployed across the continental slope off Malaga. CTD, SeaWiFS and watershed fluvial discharge data sets were also obtained from several sources to establish their relations with particle flux data.

Time-averaged fluxes for the whole period, including fluxes of organic carbon, increased slightly with depth in both locations as the result of the input of particulate matter by near-bottom nepheloid layers. Furthermore, time-averaged fluxes at mid waters were higher in the centre of the gyre than at its periphery, suggesting some kind of particle funnelling from the gyre periphery towards its centre. Temporal evolution of fluxes was highly variable throughout the year. All series showed an overall common evolution with a first peak at the beginning of summer 1997, a second broad composite peak during late autumn/winter and a third one in spring 1998. Composition of settling particles showed that summer and spring peaks were richer in biogenic constituents compared to the late autumn/winter peak.

Particle fluxes to mid water depths in the northern part of the Alboran Sea seem to be mainly controlled by fluvial discharge and primary production. Fluvial discharge could be responsible for the higher lithogenic flux during autumn and winter, while high primary production could play a key role in generating biogenic particles during spring and summer. Regarding near-bottom fluxes, the temporal evolution was controlled both by the downward transfer of particulate matter from mid waters and the advective input of mostly lithogenic and carbonate matter. The increased advective input during maximum near bottom fluxes is tentatively related to intense eddy-like activity recorded in the deep-water masses.

Keywords: Particulate flux, Continental margins, Sediment trap, Ocean circulation, Fluvial discharge, Primary production, Western Mediterranean Sea, Alboran Sea, (37°-35° N, 6°-3° W).

4.1. INTRODUCTION

The study of matter transfer between the different compartments of the marine system has been identified as one of the main scientific tasks within the MTP II-MATER project (Mediterranean Targeted Project II - MAss Transfer and Ecosystem Response). The Alboran Sea was one of the three key areas selected in the Western Mediterranean Sea for that purpose. Experiments were devised to discern the control exerted by mesoscale circulation structures, such as the Western Alboran Gyre (WAG) and the Almeria-Oran Front (AOF), on the transfer of particles to deep basin areas. The present study was undertaken in the northern half of the WAG. The reasons for choosing the Alboran Sea and the WAG were: (i) the well-known surface circulation dominated by the entrance, through the Strait of Gibraltar, of Atlantic Surface Water drawing a fluctuating anticyclonic gyre, (ii) the high productivity linked to the frontal zone associated to the northern edge of the gyre and coastal upwelling, and (iii) the scarcity of particle flux studies in that area despite its peculiar dynamical and ecological characteristics.

The Alboran Sea has long attracted the attention of physical and ecological oceanographers (see following sections for references), but only a very limited number of studies have been devoted to downward particle fluxes. Peinert et al. (1993) and Peinert and Miquel (1994) reported some flux measurements from two short-term, lagrangian flux experiments in the Eastern Alboran Gyre (EAG) and the AOF. Dachs et al. (1996, 1998) reported a detailed study of lipid compounds in settling particles collected during a 3-month trap experiment from a station located in the WAG. But neither total mass fluxes nor main constituent fluxes and the processes controlling them were discussed.

The aim of our experiment was to obtain a 1-year time series of total mass and main constituent fluxes (organic mater, calcium carbonate, biogenic opal and lithogenic fraction) along a N-S section across the northern half of the WAG (Fig. 4.1). These data were used to assess the relative contribution of factors controlling the different particle sources as well as the influence of mesoscale structures on the distribution of mid and deep-water particle fluxes.

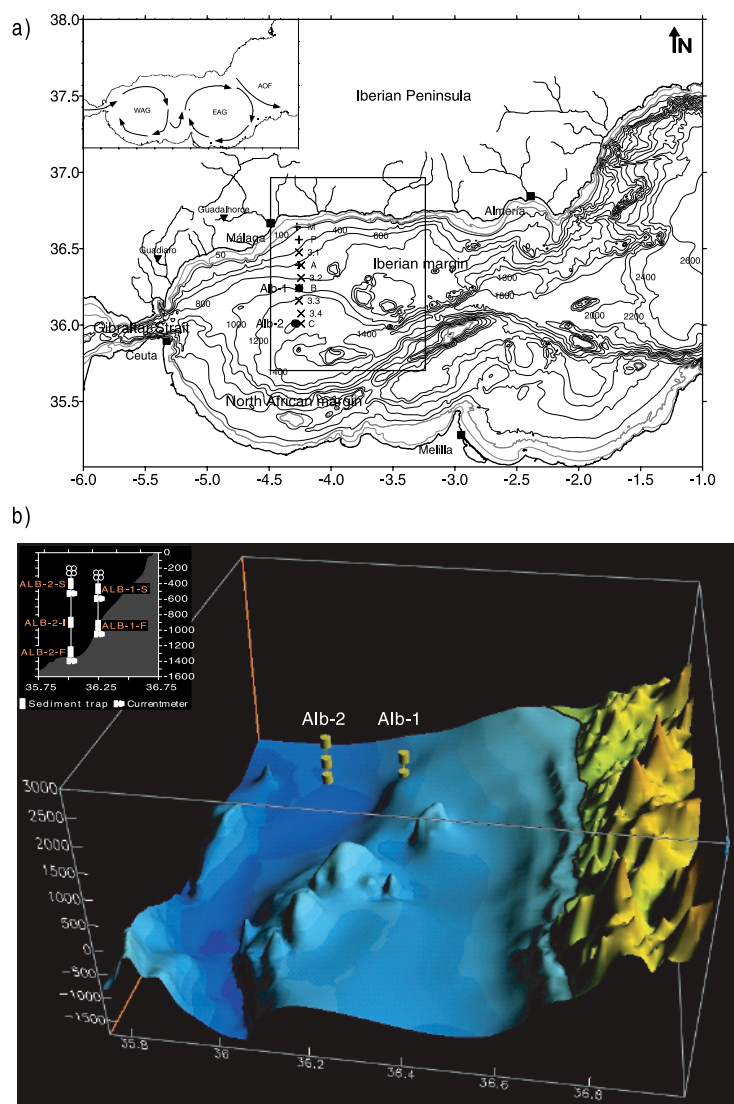


Figure 4.1. Geographical setting of the study area. a) Bathymetric map of Alboran Sea. Black dots (●) correspond to the two sediment trap-current meter stations, (X) to the 28/04/1998 CTD profiles, and (+) to the 17/09/1999 CTD profiles. Inverted triangles show the positions of the two river gauge stations considered in the discussion. The inset on the upper left corner outlines the theoretical surface circulation in Alboran Sea (WAG, Western Alboran Gyre; EAG, Eastern Alboran Gyre; AOF, Almeria-Oran Front). b) 3-D view from the ESE of the sea floor (blue tones) and coastal (green to orange) reliefs of the study area showing the location of the two mooring lines with two and three sediment trap-current meter pairs, respectively. The small inset on the upper left corner is a schematic representation of the two mooring lines. Topographic data are from the Earth Resources Information Systems Data Center (1996) and bathymetry from the British Oceanographic Data Centre (1994).

4.2. STUDY AREA

4.2.1. Physiography

The Alboran Sea, which constitutes the westernmost basin of the Mediterranean Sea, is divided into two subbasins, the Western (WAB) and Eastern (EAB) Alboran basins. The WAB, where this study was conducted, is directly connected to the Atlantic Ocean by the Strait of Gibraltar to the west. The WAB eastern boundary is roughly defined by a plateau that shows several peaks of volcanic origin and a series of sharp, NE-oriented ridges going through the Alboran Island, which is the subaerial expression of one of those ridges. Finally, the WAB is bounded by the Iberian margin to the north and the North African margin to the south. The Iberian margin, which is the closest to the study area, consists of a narrow shelf (2-10 km width, 5 km average), a wide and smooth continental slope (20-50 km width and 1:30 average gradient) and a wide base of the slope that opens into a reduced basin floor at 1400 m depth (Carter et al., 1972).

4.2.2. Physical oceanography

In contrast to the limited number of particle flux studies in the Alboran Sea there is a large set of contributions dealing with the physical oceanography of that basin for which comprehensive summaries can be found in Parrilla et al. (1986) and Heburn and La Violette (1990).

Despite its geographical location within the Mediterranean Sea, the Alboran Sea is actually a transition area between the Atlantic Ocean and the Mediterranean Sea. A 200-300 m thick jet of Atlantic Surface Water (ASW) enters the Alboran Sea from the west through the Strait of Gibraltar. The ASW is modified during its eastward migration across the Alboran Sea, becoming more saline and being mixed with Levantine Intermediate Water (LIW) of Mediterranean origin (Tintore et al., 1988). Through this process the ASW acquires salinity values between 36.48 and 36.76 psu (Sparnocchia et al., 1995) and thus becomes Modified Atlantic Water (MAW). This MAW moves into the Algerian Basin to the east, where the Almeria-Oran Front constitutes the eastern boundary of the Alboran Sea (Tintore et al., 1988). In the Alboran Sea the LIW spreads between 200-300 and 500-600 m depth, while the Western Mediterranean Deep Water (WMDW) extends underneath, down to the seafloor. The LIW core is easily recognised by its maximum salinity (>38.51 psu) and temperature (>13.07°C), higher than for MAW and WMDW (Sparnocchia et al., 1995). The densest water mass, WMDW, displays salinity values between 38.40 and 38.48 psu and

temperatures lower than 12.90°C (La Violette, 1995). Finally, in the vicinity of the Gibraltar sill, a time varying mixture of LIW and WMDW, often referred as “Mediterranean outflow” outpours into the Atlantic compensating the NAW surface inflow (Kinder and Parrila, 1987).

The MAW jet forms two anticyclonic gyres, the WAG and the EAG that dominate the circulation in the Alboran Sea (Tintore et al., 1988; Heburn and La Violette, 1990; Viudez et al., 1998). The inflowing jet initiates the WAG. According to La Violette (1984), the formation, shape and mean position of the WAG depend on (i) the physiography of the Strait of Gibraltar and the Alboran Sea, (ii) the sea surface height difference between the Atlantic Ocean and the Mediterranean Sea, and (iii) wind regimes and tides. The EAG is apparently less stable than the WAG, both in space and time, and its dynamics are less known (Millot, 1987). On the basis of several years of satellite imagery, Heburn and La Violette (1990) showed that large variations in the surface expression of these two gyres occur and that one of the gyres can occasionally disappear. The disappearance of either of the gyres takes between one and two weeks, whereas the reappearance may take between 3 weeks and two months.

4.2.3. Sources of particles

Lithogenic particles are mostly introduced to the Alboran Sea by fluvial and eolian mechanisms and, to a small extent, by coastal erosion (3-5% of the total sediment discharged into the Mediterranean Sea according to Emelyanov and Shimkus, 1986). Fluvial supply is controlled by the low and irregular precipitation throughout the year and the relatively small, arid and steep catchment areas of the rivers from its northern and southern borders (e.g. Guadiaro, Guadalhorce). Eolian supply to the Mediterranean Sea is strongly controlled by the proximity of the northern Sahara Desert and the variable southerly wind regime. Several authors have identified frequent outbreaks of dust-laden African air over the Mediterranean Sea and southern Europe and “red” and muddy rain episodes (Tomadin et al., 1984; Avila et al., 1997; Guerzoni et al., 1997). Diaz and Miranda (1997) recorded a deposition of $\sim 23 \text{ g m}^{-2} \cdot \text{y}^{-1}$ of atmospheric dust, mostly of Saharan origin, near Granada, southern Spain. Lower values, between 1 and 11 $\text{g m}^{-2} \cdot \text{y}^{-1}$, were cited by Carratala et al. (1996) and Roda et al. (1993) for the eastern coast of Spain.

Biogenic particles can be either autochthonous or allochthonous. The first are produced in the Alboran Basin by biological activity, mainly from primary production and zooplankton excretion and skeletons, whereas allochthonous biogenic particles are entrained into the basin by fluvial and eolian transport. The main phytoplankton groups in the Western Alboran Sea are dinoflagellates, nanoflagellates, diatoms, coccolitophorids and radiolarians (Delgado,

1990; Ruiz et al., 2001). Diatoms and coccolithophorids are especially important in producing, respectively, biogenic opal and calcium carbonate. Overall, the Mediterranean Sea is known to be oligotrophic, and has thus been compared to the Sargasso Sea and other central oceanic gyres (Cruzado, 1985). However, the Mediterranean Sea possesses some locally active mechanisms that enhance fertility up to mesotrophic conditions at certain periods of the year (Morel and Andre, 1991). To this respect, the Alboran Sea is one of the most productive areas within the Western Mediterranean that is not directly associated with the influence of major rivers (e.g. Ebro, Rhône, Po), urban agglomerations and/or winter intense vertical convection (e.g. Gulf of Lions and Northern Adriatic Sea). Yearly primary production estimated for the whole Alboran area by Antoine et al. (1995) reaches $200 \text{ g C m}^{-2} \text{ y}^{-1}$, the highest value for the whole Western Mediterranean Sea. Evidence of high productivity off Malaga has been provided by studies of diatom populations on surface sediments (Barcena and Abrantes, 1998). High primary production in the Western Alboran Sea is mainly associated to the local circulation pattern dominated by the WAG. Ascending nutrient transport by vertical turbulence in the Strait of Gibraltar (Packard et al., 1988), by vertical ageostrophic flow at the edge of the WAG (Ruiz et al., 2001) and by upwelling in the north-western part of the WAG (Sarhan et al., 2000), induces an enhancement of primary productivity. This enhanced productivity supports an active organic sedimentation responsible for the oxygen consumption and nutrient regeneration layer located below the photic zone (Minas et al., 1991). The dynamic control of primary productivity is therefore responsible for the temporal evolution throughout the year. Garcia-Gorriz and Carr (1999) established through the study of almost nine years of satellite derived data the annual evolution of pigment concentration in surface waters distinguishing two regimes, the bloom period between November and March, and the non-bloom period from May to September with transition periods in April-May and October-November. The same study revealed that the highest chlorophyll concentrations were located in the coastal areas of the Western Alboran Sea (north and south) and in the periphery of the WAG.

4.3. MATERIAL AND METHODS

4.3.1. Sediment traps and data recovery

Two mooring lines, ALB-1 and ALB-2, were deployed on the continental slope ($36^{\circ}15'N$, $04^{\circ}16'W$) and base of the slope ($36^{\circ}01'N$, $04^{\circ}18'W$) at 1004 m and 1337 m water depth, respectively. ALB-1 and ALB-2 mooring lines were equipped with pairs of Technicap PPS3

sediment trap and Aanderaa current meter at two and three levels within the water column (Table 4.1 and Figure 4.1). The shallowest trap - current meter pairs were located within the LIW vein at ~470 m (ALB-1-S) and \approx 400 m depth (ALB-2-S). The intermediate pair (ALB-2-I) and the near bottom pairs (ALB-1-F and ALB-2-F at 30 meters above seafloor, masf) were located within the WMDW mass. The design of the PPS3 trap (0.125 m², cylindroconical shape, 12 receiving cups), its preparation and maintenance, and the configuration of the mooring lines are described in Heussner et al. (1990). The receiving cups of the traps were filled before deployment with a 5% (v/v) formaldehyde solution in 0.45 μ m-filtered seawater. The solution was buffered by saturation with analytical grade sodium tetraborate. The poisoning solution was used to limit degradation of settled particles, and to prevent physical disruption of swimmers.

Table 4.1. Sediment trap-current meter pairs position.

Mooring line	Average position		Trap code
ALB-1	Latitude	36° 14,39' N	
	Longitude	04° 15,41' W	
	Water depth	1004	
	S trap depth	471	ALB-1-S
	F trap depth	974	ALB-1-F
ALB-2	Latitude	36° 00,63' N	
	Longitude	04° 17,49' W	
	Water depth	1337	
	S trap depth	396	ALB-2-S
	I trap depth	896	ALB-2-I
	F trap depth	1307	ALB-2-F

Locations and water depths (m) of the sediment traps and current meters deployed from June 1997 to May 1998 in the northern part of the Western Alboran Gyre.

Trap samples were obtained from July 1997 to May 1998 in three different phases: (I) 1/07/1997 - 31/10/1997, (II) 15/11/1997 - 10/03/1998 and (III) 1/04/1998 - 22/05/1998. The sampling interval was 10-11 days for the whole period except between April 20th and May 16th (within phase III) when the sampling interval was 3 days. The higher resolution data of the third period have been averaged over 9 days intervals to get a similar resolution for the whole sampling period. Results from the 3-day resolution phase will be presented in Fabres et al. (in prep.). During the whole sampling period, 157 samples were recovered out of a theoretical maximum of 180 samples, which yields an 87% success rate. Most of the sampling failures affected trap ALB-2-I, with only 17 out of 36 anticipated samples. Data from that trap have been discarded when calculating annual flux averages.

4.3.2. Sample treatment and analytical procedures

Upon recovery, trap samples were stored in the dark at 4°C until further processing in the laboratory. Following Heussner et al. (1990), the recovered samples were visually checked and the supernatant removed. Swimmers were removed by wet sieving on a 1 mm nylon mesh and hand-picking under a dissecting microscope. A high precision peristaltic pump was then used to obtain 10-20 mg sub-samples through repeated splitting of the cleaned raw samples. Sub-samples for total carbon, organic carbon and nitrogen analyses were filtered onto Millipore fibre-glass filters (APFF), while those used for mass measurement and biogenic silica analysis were filtered onto Millipore 0,45 µm cellulose filters (HA).

Total carbon, organic carbon and nitrogen content were analysed with a Fisons 1500 elemental analyser for non-treated and 25% HCl treated filters (Nieuwenhuize et al., 1994). The method to eliminate carbonate had to be slightly modified regarding the volume of HCl used because of reagent absorption by the filter. Repeated additions of 100 µl 25% HCl separated by 60 °C-drying steps were done until no effervescence was noticed. From the values obtained, organic matter (organic carbon x 2), carbonate {(total carbon – organic carbon) x 8.33} and atomic C/N values (organic carbon / organic nitrogen) were calculated. Precision and accuracy of the carbon and nitrogen measurements were checked against the Canadian National Research Council certified estuarine sediment MESS-1 (Berman, 1990). Short term precision of carbon and nitrogen (n = 8) averaged ± 2.3% and ± 5.0% of the measured values respectively. Mid term precision over the period between March and May 2000 (n=24) was ± 2.9% for carbon and ± 8.4% for nitrogen. The accuracy of the method is excellent as indicated by the correspondence between the measured carbon values, $3.05 \pm 0.04\%$, and the certified carbon values of the standard, $2.99 \pm 0.09\%$. The uncertainties in the accuracy values lie within 95% confidence limits.

Since our samples hold particularly low silica contents, it was necessary to implement a new analytical method. The method derives from the procedure described by Mortlock and Froelich (1989) regarding the use of Na₂CO₃ solutions for the extraction of amorphous silica. Nevertheless, it has been modified substantially by: (i) incorporating a two step leaching with 0.5 M Na₂CO₃ (2.5 hours each) separated by filtration of the leachate, (ii) using Inductive Coupled Plasma Atomic Emission Spectroscopy (ICP-AES) for the analysis of Si (Fabres et al., 2000) and Al content, and (iii) correcting the Si contents of the first leachate by means of the Si/Al relation of the second one (Kamatani and Oku, 2000). Corrected Si concentrations are transformed into biogenic opal concentrations by multiplying the obtained values by a factor of 2.4 (Mortlock and Froelich, 1989).

Twenty ml of 0.5 M Na₂CO₃ are added in a polypropylene tube to an HA filter containing an aliquot of 10-20 mg of sediment. The tube is stirred and sonicated for 5 minutes. Subsequently the tube is left in a thermostatic bath for 2.5 h at 85°C, stirring again after 1 and 2 h. Without any delay after the removal from the thermostatic bath, the solution is filtered onto an HTTP Millipore filter using an all plastic filtering apparatus. The filter with all the remaining particles is dried at 60°C during 12 h. The same procedure described above is repeated over the HTTP filter in order to obtain a second leachate. The only difference is that at the end of the 2.5 h the supernatant is separated from the solid residue by centrifuging at 6000 rpm during 5 minutes. The solution obtained from each leaching process is diluted 1/10 immediately after cooling down to ambient temperature. This dilution step is implemented to reduce the Na concentration in the final solution that has to be analysed. Finally, Si and Al concentration in both solutions are determined through Inductive Coupled Plasma Atomic Emission Spectroscopy (ICP-AES) using a Thermo Jarrell Ash spectrometer. Short term precision of opal measurements averaged 4.5% of the measured values and was determined from replicate analysis (n = 3 or 4) of seven trap samples that covered a broader range of compositions than those of the analysed samples (1.07%-14.70%).

Lithogenic fluxes are calculated applying the formula: lithogenic flux = total flux – biogenic flux, considering the biogenic flux = organic matter flux + carbonate flux + opal flux. Mean fluxes were calculated using the data between July 1997 and May 1998.

4.3.3. Current meter data and hydrological profiles

Aanderaa RCM-7/RCM-8 current meters were deployed together with surface (S) and bottom (F) traps to record at an hourly frequency current speed and direction. Table 4.2 shows the total number of recorded days for each current meter and the concerned deployment periods. The ALB-2-F current meter properly recorded the direction but not the speed and therefore no speed or residual direction could be obtained from the record. The hourly data have been low-pass filtered with a cut-off period of 2 days to remove the tidal oscillations and highlight the subinertial oscillations of lower frequency (Plaza, 2001).

Water column characteristics were recorded during two multidisciplinary cruises on board R/V Hesperides in April 1998, at the end of the study period, and September 1999. Hydrological profiles were recorded using CTD Neils Brown Mark III and Mark V profilers coupled with a Sea Tech 25 cm pathlength, 660 µm wavelength transmissometer. Light transmission data presented here correspond to raw output voltage, which is merely a qualitative expression of the amount of particles in the water column. The CTD data have been used to construct two N-S transects off Malaga through the two mooring lines (Fig.

4.1a) that illustrate the contrasting spring and autumn hydrological structures of the area. The WAG was fully developed in April 1998 but was hardly detectable in September 1999.

Table 4.2. Current meter data.

Current meter	Recorded days	Average speed ± stand. dev. (cm s ⁻¹)	Maximum speed (cm s ⁻¹)	Percentage values > 12 cm s ⁻¹	Residual direction (degrees from N)	Residual speed (cm s ⁻¹)
ALB-1-S	231 (I, II)	3.70 ± 2.13	12.72	0.1 %	272.01	1.93
ALB-1-F	332 (I, II, III)	4.96 ± 3.29	22.31	3.5 %	273.91	2.74
ALB-2-S	199 (I, III)	4.17 ± 2.36	13.89	0.2 %	101.64	0.95

Average and maximum speed, percentage of individual measurements above 12 cm s⁻¹, and residual speed and direction for the periods recorded by each current meter.

4.3.4. SeaWiFS satellite images and fluvial discharge time series

SeaWiFS (Sea-viewing Wide Field-of-view Sensor) images of chlorophyll-a concentration (chl-a mg m⁻³) were obtained from the Marine Environment Unit of the Space Applications Institute (Joint Research Centre, European Commission) (Melin, 2000). The series of 10-day composite images covers the whole Alboran Sea. Each individual scene is mapped onto geographical grids of 2 km resolution (Melin et al., 2000).

Daily fluvial discharges (m³ s⁻¹) corresponding to the study period have been obtained from the “Confederación Hidrográfica del Sur” for the two main rivers, Guadiaro and Guadalhorce, which pour their waters west of our experimental site (Fig. 4.1a). It is assumed that the anticyclonic circulation in the WAG deflects eastwards the inputs from these two rivers. The chosen gauge stations belong to those affluent rivers unaffected by dam regulation that are the nearest possible to the mouths of the Guadiaro and Guadalhorce rivers (Fig. 4.1a).

4.4. RESULTS AND DISCUSSION

4.4.1. Hydrodynamic conditions

Table 4.2 displays basic statistics for speed and direction recorded by each current meter. Figure 4.2 displays scattergrams of instantaneous current measurements. At ALB-1 the residual water flow is oriented towards the W throughout the water column (272°-274°) with an average near-bottom speed (~2.7 cm s⁻¹) higher than in the intermediate layer (~1.9 cm s⁻¹). Currents recorded at ALB-2 present more variable directions. In the intermediate layer the

residual speed is $\sim 1 \text{ cm s}^{-1}$ towards the E (102°). Only directions are available near-bottom at ALB-2. Two approximately equally distributed directions are observed, ESE (110°) and WSW (247°) which probably result from the influence of bottom topography (data not shown).

These limited observations extend and confirm previous field measurements performed in the area. Pistek et al. (1985) recorded, during three months in 1982 between 220 and 1100 m depth, a weak coherent cyclonic motion whose vortex was located at about 35.75° N , 4.25° W , i.e. close to the position of ALB-2. In a N-S section located westward of our study area, Parrilla et al. (1986) recorded a mean flow of $1.2\text{-}2.3 \text{ cm s}^{-1}$ and W-WSW directions at 540 m depth. Mid and deep-water residual speeds and directions at ALB-1 agree with that general cyclonic circulation with westward flow of the intermediate and deep waters along the Spanish slope. The eastward steady flow recorded in the intermediate water column at ALB-2 could be the result of the proximity of this mooring to the centre of the cyclonic deep gyre, considering that a slight time-varying northward shift on its position could easily result in an eastward residual flow.

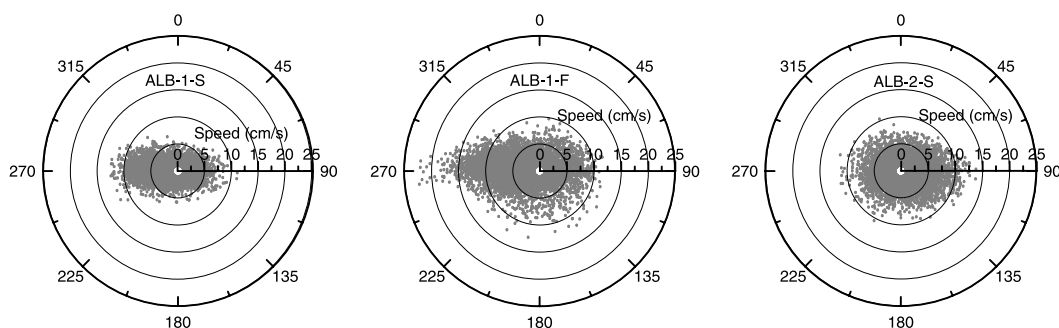


Figure 4.2. Scattergrams for all the instantaneous current data recorded by each current meter. Speed/direction scatter plot for ALB-2-F is not available. Speed is in cm s^{-1} and direction in degrees from N.

Trap collection efficiency has been questioned because of potential hydrodynamic bias at high current speeds (Baker et al., 1988; Gust et al., 1992, 1994; Gardner et al., 1997) and errors due to trap tilting (Gardner, 1985). Taking into account the reduced time during which individual speed measurements exceeded 12 cm s^{-1} (Table 4.2), the empirical threshold determined by Baker et al. (1988) beyond which collection efficiency of a cylindrical trap was considerably reduced, we consider that hydrodynamic biases were negligible. Furthermore, Gardner et al. (1997) showed that fluxes collected with traps having a diameter and an aspect ratio very similar to ours (30.5 cm and 3 compared with 40 cm and 2.5 for the PPS-3) were only slightly biased at current speeds as high as 22 cm s^{-1} . Therefore, the threshold speed of 12 cm s^{-1} is a very conservative limit. Finally, deployment depths of the

traps determined by current meter pressure sensors decreased slightly at the beginning of the first deployment due to the stretching of the mooring line and remained constant afterwards, with no periodic oscillations. This indicates that the moorings remained in vertical position throughout the whole experiment and that tilting bias may be considered negligible as well.

4.4.2. Spatial distribution of mean composition and fluxes of settling particles

The average composition of settling particles is largely dominated by the lithogenic fraction (Figure 4.3 and Table 4.3). Its contribution to total flux is slightly higher in ALB-2 traps, around 76 %, than in ALB-1 traps, around 69%. These values are remarkably constant with depth at each mooring site. On the contrary, the contributions of organic matter and biogenic opal decrease with depth while the contribution of carbonate increases. Atomic C/N ratios, ranging from 7.07 to 8.49, are similar to values previously determined for organic matter collected in Mediterranean trap experiments (Buscail et al., 1990; Miquel et al., 1994; Miserocchi et al., 1999). It is worthy to note that the lowest value is observed in the shallow trap of ALB-2. Furthermore, the ratios increase with depth, a situation that illustrates organic matter degradation during its transfer to deeper areas of the margin (Buscail et al., 1990).

Mean total mass fluxes show a limited spatial variability and range from 503 mg m⁻² d⁻¹ in the ALB-1 upper trap to 855 mg m⁻² d⁻¹ in the ALB-2 near-bottom trap (Figure 4.3 and Table 4.3). Such values lie on the lower side of the range of total mass fluxes measured in various locations of the Northwestern Mediterranean basin. They are similar to values given for the entrance of the Gulf of Lions (Heussner et al., 1996; Monaco et al., 1999), but much lower than the several g m⁻² d⁻¹ recorded at the exit of the Gulf of Lions (Monaco et al., 1990; Heussner et al., 1996) or in the Catalan Sea (Puig and Palanques, 1998a). The latter areas are, however, strongly affected by the outflow of major rivers (Rhône and Ebro) and the channelling effect of canyons. The observed differences in total mass may therefore already indicate that the processes controlling particle transfer on the WAB continental slope could be different from those identified in other margins of the Western Mediterranean. We will now examine the main compositional and quantitative trends of particle fluxes to better understand these processes.

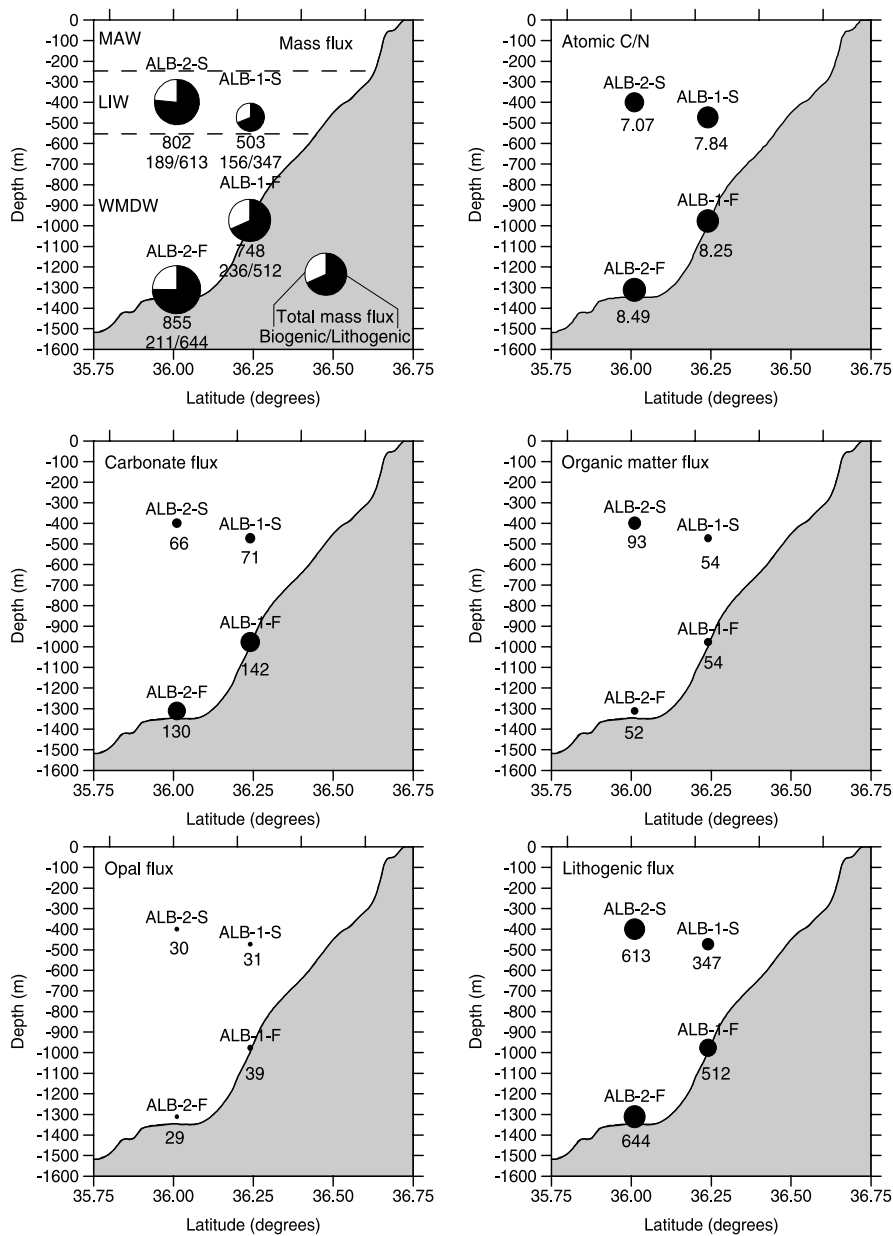


Figure 4.3. Time-weighted fluxes of total mass, fluxes of main constituents and atomic organic C/N ratio of settling particles collected in the WAB. Dots are proportional to values. Flux values below each dot are in mg·m⁻²·d⁻¹. Lithogenic fluxes in the pie charts appear in black and biogenic fluxes (carbonate + organic matter + opal) in white. MAW, Modified Atlantic Water; LIW, Levantine Intermediate Water; WMDW, Western Mediterranean Deep Water.

Table 4.3. Time averaged fluxes and main constituents percentages.

Trap code (<i>n</i> samples)	Mass Flux $\text{mg m}^{-2} \text{day}^{-1}$	Total C $\text{mg m}^{-2} \text{day}^{-1}$ (%)	Organic C $\text{mg m}^{-2} \text{day}^{-1}$ (%)	Organic N $\text{mg m}^{-2} \text{day}^{-1}$ (%)	C/N	CaCO ₃ $\text{mg m}^{-2} \text{day}^{-1}$ (%)	Org. Matter $\text{mg m}^{-2} \text{day}^{-1}$ (%)	Opal $\text{mg m}^{-2} \text{day}^{-1}$ (%)	Lithogenic $\text{mg m}^{-2} \text{day}^{-1}$ (%)
ALB-1-S (36)	502.76	35.41 (7.04%)	26.90 (5.35%)	4.00 (0.80%)	7.84	70.88 (14.10%)	53.79 (10.70%)	31.31 (6.23%)	346.77 (68.97%)
ALB-1-F (36)	748.42	44.32 (5.92%)	27.23 (3.64%)	3.85 (0.51%)	8.25	142.36 (19.02%)	54.47 (7.28%)	39.40 (5.26%)	512.19 (68.44%)
ALB-2-S (32)	802.36	54.61 (6.81%)	46.63 (5.81%)	7.69 (0.96%)	7.07	66.44 (8.28%)	93.26 (11.62%)	29.58 (3.69%)	613.07 (76.41%)
ALB-2-F (36)	854.86	41.58 (4.86%)	26.00 (3.04%)	3.57 (0.42%)	8.49	129.77 (15.18%)	52.01 (6.08%)	28.94 (3.39%)	644.14 (75.35%)

Time-averaged fluxes of total mass and main constituents ($\text{mg m}^{-2} \text{d}^{-1}$) and relative contributions (%) of main constituents to total mass for the ALB-1-S, ALB-1-F, ALB-2-S and ALB-2-F traps.

Two major features dominate the spatial distribution of mass fluxes. First, it can be observed that mean total mass fluxes increase with depth at both stations, though the increase is only significant at ALB-1 (x 1.5). This increase largely results from a flux increase of the lithogenic component of settling particles and, to a lesser extent, of carbonate. This vertical trend, observed on most continental slopes, is usually explained by the advective input of particles, e.g. through detached or near-bottom nepheloid layers loaded with lithogenic and carbonate-rich particles (Heussner et al., 1999 and references therein). The two N-S hydrographic transects through the mooring lines performed in 1998 and 1999 clearly show higher particle concentrations around the two near-bottom traps, especially during the April 1998 survey (Fig. 4.4). The development of a bottom nepheloid layer around the position of ALB-1-F is probably linked to the impinging of a density front (see temperature sections in Figure 4.4) close to a slope gradient break. This gradient break is located at around 950 m depth and forms the edge of the volcanic plateau and seamounts east of the study area (Fig. 4.1b). Resuspension of bottom sedimentary particles by the interaction of dynamic processes with hydrographic structures in the proximity of bottom irregularities has been documented by several authors elsewhere (Palanques and Biscaye, 1992; Puig and Palanques, 1998b; Durrieu de Madron et al., 1999). The slightly enhanced particle flux to the deepest trap ALB-2-F probably originates from the focussing of particles settling from nepheloid layers issuing from the surrounding margins or seamounts. Such a mechanism has been proposed, amongst others, by Huang and Stanley (1972) to explain the higher sedimentation rates during the Holocene on the deepest areas of the WAB.

The second striking feature of the distribution of mean mass fluxes is the higher flux recorded by the shallow trap at ALB-2 ($802 \text{ mg m}^{-2} \text{ d}^{-1}$) compared to its counterpart at ALB-1 ($503 \text{ mg m}^{-2} \text{ d}^{-1}$). This difference first results from a much higher lithogenic flux at ALB-2, and secondarily from differences in organic matter (Fig. 4.3 and Table 4.3). Such a seaward flux distribution is rather unusual for continental margins where fluxes at a given depth generally decrease with distance from the shelf break (e.g. Heussner et al., 1999). Let us examine in detail the different mechanisms that could be invoked to explain this "inverted" horizontal distribution. First, the difference could arise from the depth difference between the two traps. Indeed, the ALB-1-S trap was deployed 70 m deeper than ALB-2-S and could therefore show a lower organic matter flux due to particle degradation. To check this possibility we use the relation of Martin et al. (1987) describing the vertical distribution of particulate organic carbon flux:

$$F = F_d(z/d)^{-0.858} \quad (4.1)$$

where F is the organic carbon flux calculated at depth z and F_d is the organic carbon flux measured at depth d . Extrapolating the organic carbon flux at site ALB-1 from 470 m to 400 m yields a value of $32.6 \text{ mg m}^{-2} \text{ d}^{-1}$ that is still 14 mg lower (30%) than the corresponding flux at ALB-2. Degradation is not sufficient to account for the observed differences between the two sites and we have therefore to seek for eventual differences in the biological sources of material that feed both traps. From the set of chlorophyll-*a* concentration images presented in section 4.4.3.1 (Fig. 4.8), but also from the nine years of satellite derived data presented by Garcia-Gorriz and Carr (1999), it is clear that surface primary production is, on average, higher at the northern periphery of the WAG. This is exactly the opposite situation that could be expected if the flux differences were to reflect production differences in the waters overlying the traps. The fact that neither increased outputs (degradation) nor inputs (production) are able to provide a satisfactory explanation leads us to consider a less documented, more complex dynamical mechanism. The higher particle flux to the ALB-2-S trap could result from the funnelling or “subduction” of surface waters and particles from the periphery of the WAG towards its centre. The surface, highly productive waters located north of the gyre are pushed towards the edge of the gyre by offshore blowing winds or the shift towards the south of the Atlantic jet (Sarhan et al., 2000). Meeting the lighter waters of the Atlantic jet these waters subduct below them, entraining surface generated particles along isopycnals. Part of these particles are probably entrained in the jet by turbulent mixing and ageostrophic vertical motions and swept away eastwards. However the remaining particles could be advected south- and downward along isopycnals before reaching the central area of the gyre where the less dynamic environment favours particle flocculation, aggregation and sinking. The hypothesis of enhanced particle transfer towards the centre of the gyre has been first postulated by Packard et al. (1988) to explain the formation and maintenance of an oxygen minimum zone in subsurface waters in the WAB. Isopycnal particle transfer has also been proposed to explain increased downward fluxes at depth in EAB waters located outside the main path of the productive Atlantic jet waters (Peinert and Miquel, 1994). Finally, subduction of dense waters below the frontal structure associated with the Atlantic jet in the WAG has been recently suggested by Gomis et al. (2001). Several of our own observations further support this mechanism. Particle concentration sections in Figure 4.4 clearly illustrate the process, and show that it is more active when the gyre is well established (April 1998) and there is a strong density front in surface. The C/N ratio mean value at ALB-2-S (7.07) is lower than at ALB-1-S (7.84), but very close to the average values reported for particles collected at 250 m depth at the centre of the WAG (6.70) (Dachs et al., 1996), confirming the enhanced transfer of fresh organic matter towards the centre of the gyre. Concomitantly with the enhanced organic matter flux there is as well an enhanced flux of lithogenic particles.

This may be the result of the formation of particle aggregates in the periphery of the gyre - thus near the coast where lithogenic particle concentration in surface waters may be substantial - and their funnelling towards the centre of the gyre.

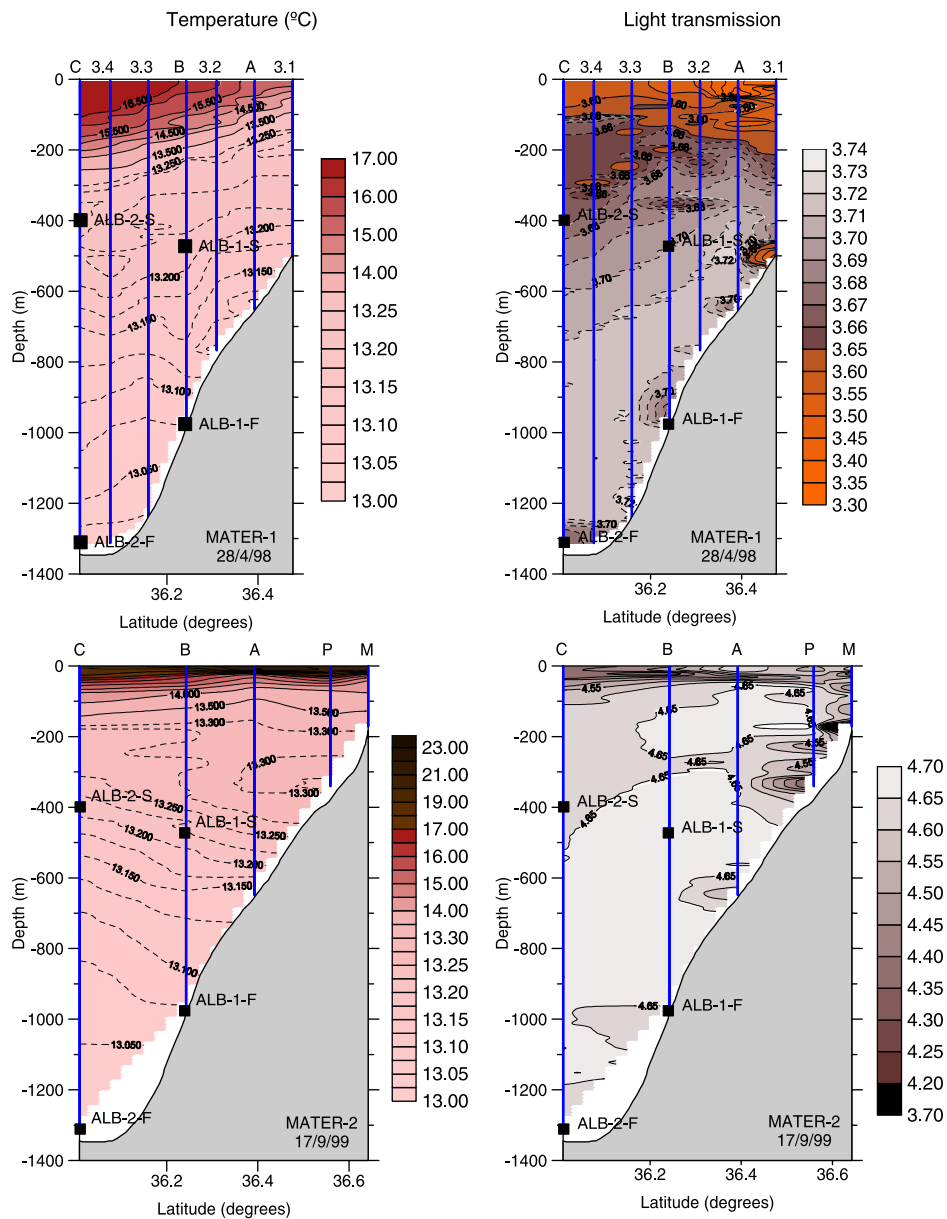


Figure 4.4. Temperature (°C) and light transmission transects off Malaga across the mooring positions in April 98 and September 99. Vertical bold lines represent the CTD casts located in Figure 4.1a. Light transmission is given as raw output voltages with a different scale for each transect.

4.4.3. Temporal evolution of total mass and major constituents fluxes

Table 4.4 and figures 4.5 and 4.6 summarise the fluxes and concentrations of total mass and main constituents of all samples. Total mass fluxes fluctuate at least by one order of magnitude from the minimum to the maximum in each trap. The highest flux is recorded in ALB-2-S ($2026 \text{ mg m}^{-2} \text{ d}^{-1}$) and the lowest in ALB-1-S ($30 \text{ mg m}^{-2} \text{ d}^{-1}$). Since fluctuations of total mass fluxes extend over several orders of magnitude while percentage contributions of all constituents evolve within a narrow range, fluxes of each of the main constituents essentially match the temporal evolution of total mass flux. Temporal flux variability of these constituents is therefore high, as indicated by coefficients of variation (C.V.% = standard deviation/mean x100) above 50% for mass fluxes and constituents in all traps (Table 4.4). Leaving aside ALB-2-I, whose statistics may be biased due to under-sampling (cf. section 4.3.1), ALB-2-S is the trap that records the highest variability. However, a common overall evolution can be observed in all traps, with a peak at the beginning of the summer, a broad composite peak during late autumn and winter and a third peak in spring. Minimum values are reached at the end of August, beginning of September, and from mid February to mid March (Figs. 4.5 and 4.6). A careful comparison between the temporal series (total mass fluxes and percentages of main constituents) in mid water (ALB-1-S, ALB-2-S and ALB-2-I) and near-bottom traps (ALB-1-F and ALB-2-F) reveals a much more synchronous evolution within each set. This observation suggests that the timing of the processes controlling particle fluxes at mid water depths or in near-bottom waters could differ and, therefore, that the control processes may be, at least partly, different.

Table 4.4 Descriptive statistics for each temporal series of fluxes and main constituent composition

Statistics	Mass flux	Total carbon		Organic carbon		Organic nitrogen		Corg/Norg		Carbonate		Organic matter		Opal		Lithogenic	
		%	flux	%	flux	%	flux	%	flux	%	flux	%	flux	%	flux	%	flux
Maximum	1137.07	12.95	89.91	12.17	81.70	1.91	13.74	9.49	21.00	207.54	24.33	163.41	13.56	93.07	82.49	896.74	
Minimum	29.79	4.58	3.86	2.90	3.13	0.4	0.51	6.45	3.02	5.20	5.79	6.27	1.28	1.32	54.23	16.15	
ALB-1-S Mean	513.71	7.69	37.24	6.06	28.44	0.92	4.25	7.84	13.52	73.25	12.13	56.89	6.06	31.79	68.22	365.31	
Std. Dev.	298.07	2.24	20.39	2.40	16.84	0.40	2.64	0.76	5.53	57.48	4.79	33.68	2.87	25.03	7.18	209.34	
C.V. (%)	58.02%	29.16	54.76%	39.52	59.21%	43.93	62.12%	9.75%	40.90	78.47%	39.52	59.21%	47.38	78.73%	10.52	57.30%	
Maximum	1702.58	9.08	94.28	5.97	67.38	1.02	11.18	9.14	39.55	298.31	11.93	134.77	9.36	113.64	80.65	1302.27	
ALB-1-F Minimum	245.08	4.24	13.98	2.43	7.85	0.34	1.09	6.83	6.66	30.14	4.87	15.71	1.83	8.04	47.38	145.02	
Mean	764.36	6.13	45.45	3.74	28.31	0.53	4.01	8.31	19.90	142.73	7.48	56.63	5.03	40.19	67.58	524.82	
Std. Dev.	425.43	1.08	24.41	0.84	17.28	0.15	2.51	0.58	7.41	77.48	1.68	34.56	2.02	32.32	7.94	313.64	
C.V. (%)	55.66%	17.57	53.71%	22.24	61.03%	29.01	62.56%	6.99%	37.22	54.29%	22.41	61.03%	40.13	80.42%	11.75	59.76%	
Maximum	2025.81	12.15	114.92	10.08	104.79	1.56	19.73	9.38	19.00	277.12	20.16	209.59	14.42	72.97	86.38	1703.99	
ALB-2-S Minimum	32.12	4.71	3.95	3.74	3.73	0.52	0.53	6.03	0.00	0.00	7.48	7.46	1.38	0.77	48.21	43.98	
Mean	803.07	7.56	56.74	6.36	48.19	1.01	7.90	7.43	10.03	71.19	12.71	96.39	4.66	29.67	72.51	635.51	
Std. Dev.	599.86	2.13	33.18	1.79	29.84	0.29	5.40	0.94	6.80	69.50	3.57	59.68	3.29	19.84	10.89	503.02	
C.V. (%)	74.69%	28.23	58.49%	28.12	61.91%	28.90	68.38%	12.65%	67.81	97.62%	28.12	61.91%	70.65	66.87%	15.02	79.15%	
Maximum	960.46	12.67	82.22	10.90	80.62	2.22	16.43	8.77	20.32	136.70	21.80	161.24	12.51	49.03	78.91	698.65	
ALB-2-I Minimum	102.84	5.14	10.04	3.96	8.02	0.61	1.19	5.72	1.80	13.32	7.92	16.03	3.59	6.13	47.01	63.84	
Mean	436.02	8.14	33.43	6.53	27.06	1.08	4.68	7.20	13.29	52.92	13.06	54.12	5.84	23.13	67.81	305.85	
Std. Dev.	295.91	2.37	23.19	2.44	21.97	0.47	4.52	0.86	5.07	40.35	4.88	43.93	2.67	14.39	8.36	220.48	
C.V. (%)	67.87%	29.16	69.36%	37.38	81.18%	43.79	96.41%	11.91%	38.12	76.25%	37.38	81.18%	45.70	62.20%	12.34	72.09%	
Maximum	1935.36	8.29	105.04	7.92	76.24	1.39	9.91	9.39	19.95	256.17	15.83	152.49	10.75	143.16	81.47	1574.26	
ALB-2-F Minimum	67.93	3.57	7.57	2.07	3.11	0.29	0.39	6.64	3.12	8.05	4.14	6.22	1.42	1.56	59.78	84.12	
Mean	867.10	5.24	43.76	3.48	26.60	0.48	3.65	8.53	15.02	136.20	6.95	53.20	3.54	29.63	74.52	673.04	
Std. Dev.	535.59	1.21	23.50	1.28	15.27	0.21	2.04	0.58	3.32	78.99	2.57	30.55	1.85	25.60	4.80	414.33	
C.V. (%)	61.77%	23.08	53.69%	36.95	57.42%	43.84	55.95%	6.82%	22.12	57.99%	36.95	57.42%	52.14	86.41%	6.45	61.56%	

 Descriptive statistics of total mass and main constituent fluxes ($\text{mg m}^{-2} \text{d}^{-1}$), C/N ratios, and contribution (%) of main constituents to total mass for the different traps

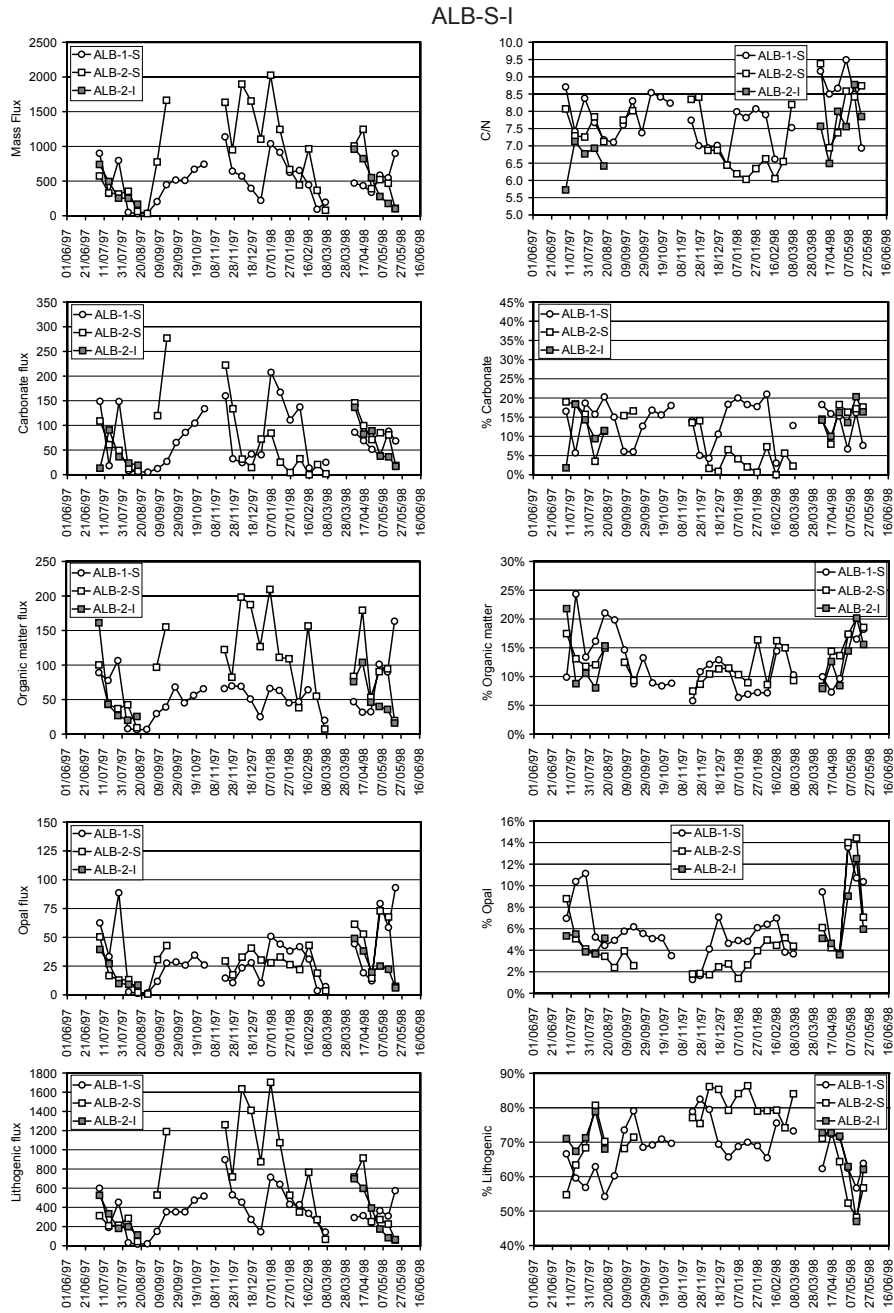


Figure 4.5. Temporal evolution of total mass fluxes ($\text{mg m}^{-2} \text{d}^{-1}$), fluxes and percentages of main constituents, and atomic C/N ratios for the shallow and intermediate sediment traps.

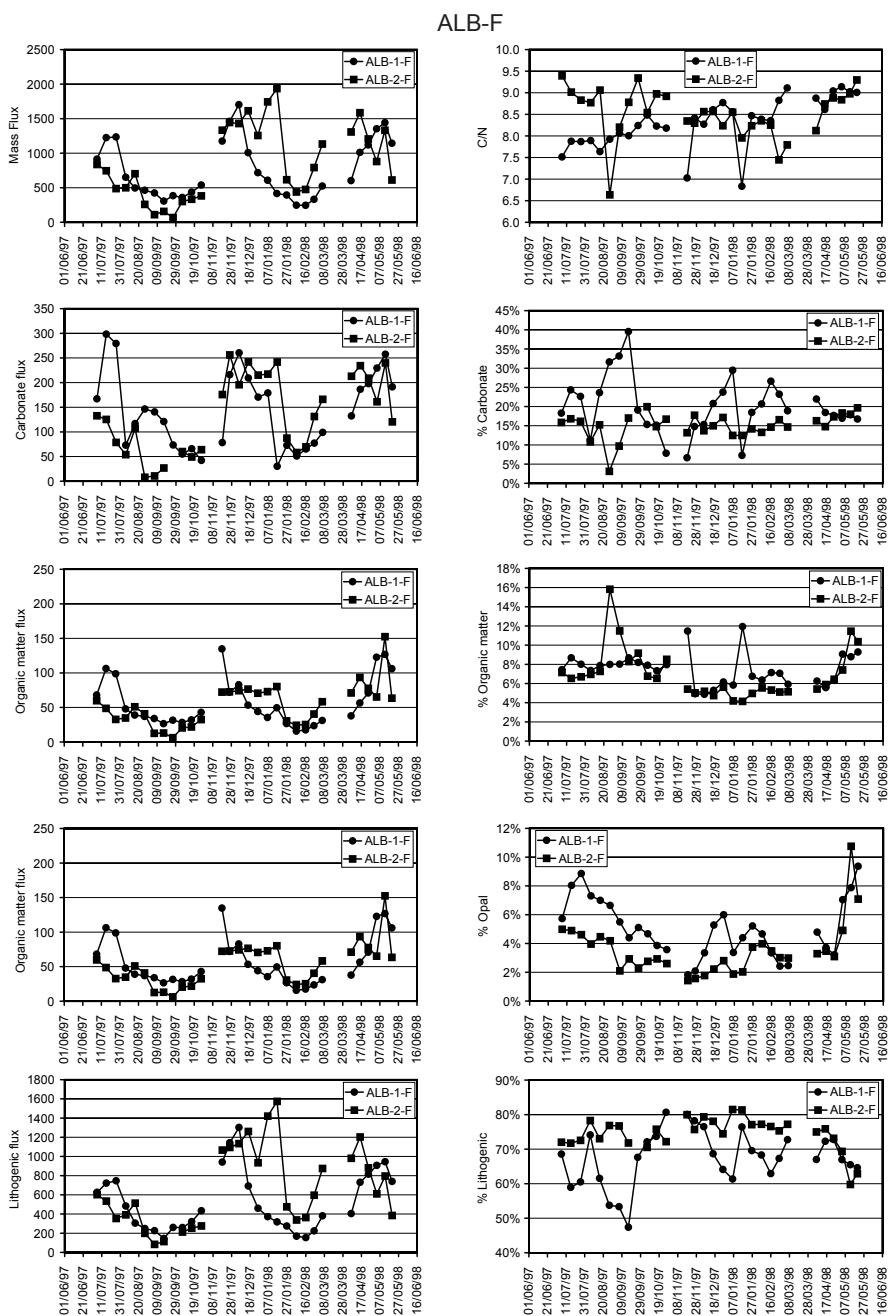


Figure 4.6. Temporal evolution of total mass fluxes ($\text{mg m}^{-2} \text{d}^{-1}$), fluxes and percentages of main constituents, and atomic C/N ratios for the sediment traps located at 30 m above the sea floor.

4.4.3.1. Temporal evolution of fluxes to mid water depths

Particle fluxes at mid water depths (Fig. 4.5) are characterised by higher values during autumn-winter than in spring and at the end of summer. Particles settling at the end of summer and during spring peaks are relatively rich in organic matter and biogenic silica, poor in lithogenic fraction and within average in carbonate contents. The composition of the autumn-winter peak is more heterogeneous, both spatially and temporally. On average, particles settling during that period have a stronger lithogenic component and contain less organic matter and biogenic silica. Carbonate weight percentages are high in the peaks recorded in the ALB-1-S trap while they fluctuate between high and very low in the peaks recorded from autumn to winter in the ALB-2-S trap. The compositional evolution of fluxes to mid water depths responds to the different sources and origins of the particles that settle through the water column. A good coincidence is observed in the winter timing of river flow events and high chlorophyll-a concentrations, suggesting that the arrival of nutrient-rich fresh waters to shelf areas of WAB fertilises surface waters. This phenomenon has been observed in other areas (Salisbury et al., 2001) and could complement other mechanisms such as circulation-induced upwelling in the triggering of phytoplankton blooms. High concentrations of lithogenic and biogenic particles in surface waters during winter blooms would then favour the formation of aggregates, contributing thus to the enhanced export of particles towards deeper waters.

A first control is thus exerted by the input of allochthonous lithogenic particles by river discharges in the north-western coast of the WAB. Comparison of lithogenic fluxes with the evolution of Guadiaro and Guadalhorce river flow (Fig. 4.7) reveals that the mid-winter lithogenic flux peaks are preceded, with an anticipation of 10 to 20 days, by peaks in river flows. However, there is no linear relationship between the magnitudes of particle fluxes and river flow peaks. The first river surges, from late September to late November 1997, are modest, while the corresponding flux increases are quite drastic. In contrast, the last noticeable surge at the beginning of February 1998 seems to have little effect on lithogenic fluxes. That imbalance between river flow and lithogenic fluxes may result from the erosive regime in arid watershed areas, which are generally characterised by an increased solid discharge at the onset of the wet season (e.g. Martins and Probst, 1991; Eisma, 1993). The importance of riverine particle inputs during autumn and winter also explains the overall higher particle fluxes recorded during that period compared to spring and summer. Eolian input of lithogenic material probably plays only a limited role since average dust fluxes recorded in Granada by Diaz and Miranda (1997) (c.a. $60 \text{ mg m}^{-2} \text{ d}^{-1}$) are one order of

magnitude lower than the lithogenic fluxes recorded in ALB-1 and ALB-2 shallow traps (Fig. 4.3).

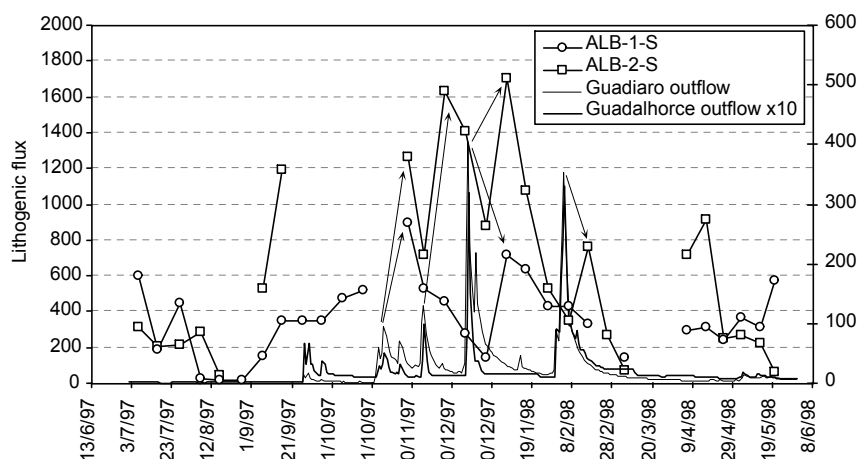


Figure 4.7. Temporal evolution of lithogenic fluxes ($\text{mg m}^{-2} \text{d}^{-1}$) at the two shallow traps and Guadiaro and Guadalhorce river flows ($\text{m}^3 \text{s}^{-1}$).

The second important mechanism controlling particle fluxes to mid water depths is primary production that provides organic matter, carbonate and biogenic silica particles. SeaWiFS chlorophyll-a images averaged over 10-day periods (Fig. 4.8) show the temporal evolution of biological productivity for the whole WAG area that can be compared with organic matter fluxes in shallow traps (Fig. 4.9). Disregarding their magnitude, the flux peaks present a similar synchronous evolution in both traps. It is further noticeable that these peaks appear 10 to 30 days after production events in surface waters of the WAG, indicated by increased chlorophyll concentrations. The delay in vertical transfer for both river-contributed lithogenic particles and primary production derived particles allow a rough estimate of transfer speeds in the range of $13\text{-}50 \text{ m d}^{-1}$, e.g. at the lower end of previously published values (see review by Siegel and Deuser, 1997).

Capítol 4. Composition and variability of fluxes in the Western Alboran Sea

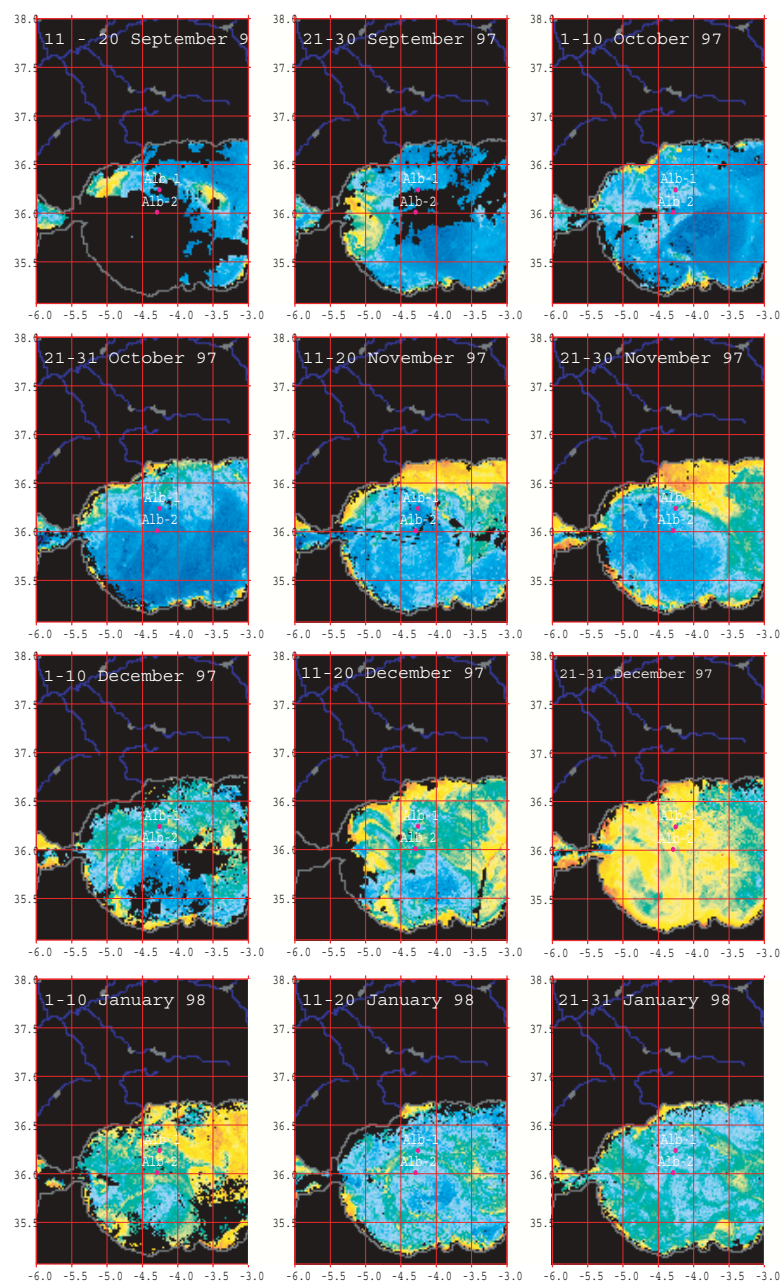


Figure 4.8. Chlorophyll-a concentrations for the Western Alboran Sea between mid-September 1997 and May 1998. SeaWiFS images are averaged over periods of 10 days. Red dots correspond to the location of the two mooring lines. Two periods for which cloud coverage over the study area was too high are not shown.

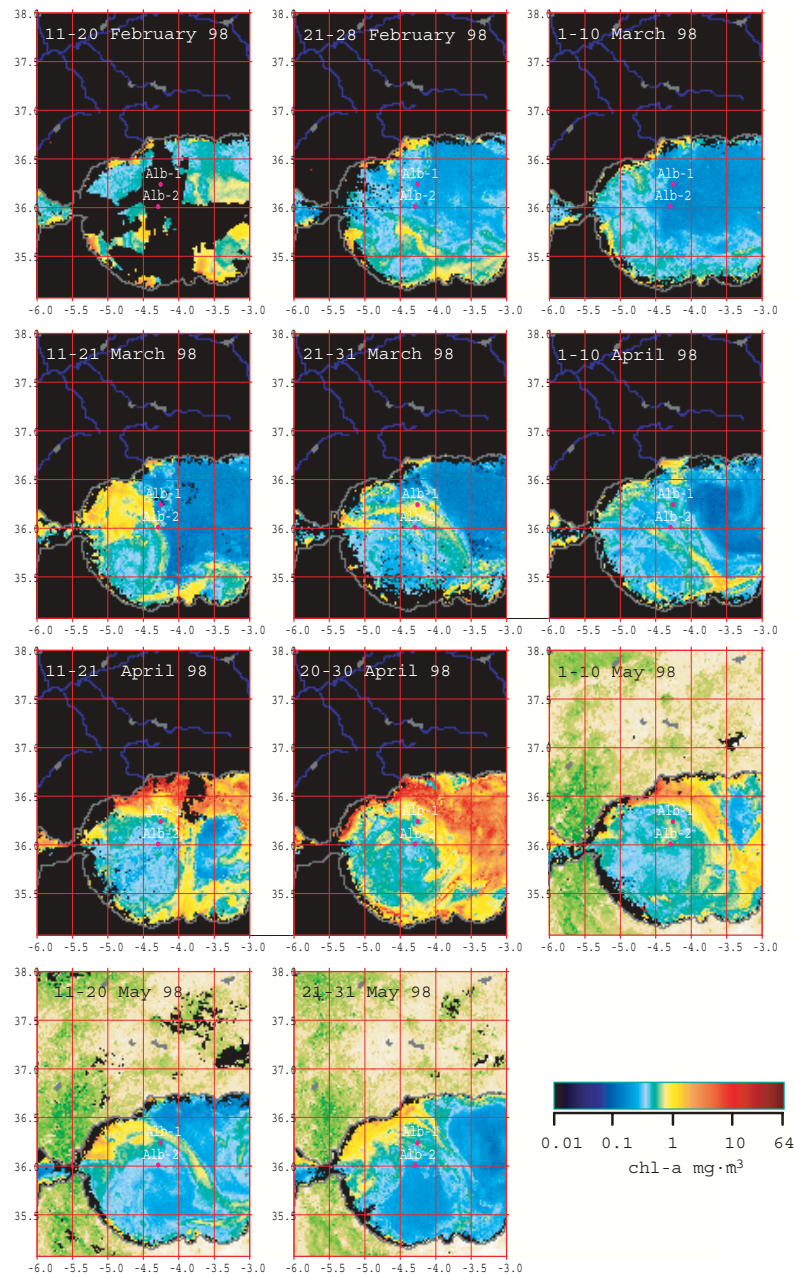


Figure 4.8. Continued

There is at least one clear exception to the general synchronous evolution of organic matter flux to both shallow traps. During the last sampling period of April-May 1998 there is a drastic increase of total mass and organic matter flux in ALB-1-S while flux to ALB-2-S is

clearly decreasing. The shape and position of the WAG during that period may cause that exception. At that period, WAG is elongated in a N-S direction and, therefore, maximum production develops very close to the coast (see the 21-31 May chlorophyll image in Fig. 4.8), allowing an enhanced biogenic particle flux to reach ALB-1-S but not ALB-2-S. The analysis of higher resolution records obtained during this sampling period (Fabres et al., in prep.) will probably allow a finer interpretation of spatio-temporal variability in particle fluxes.

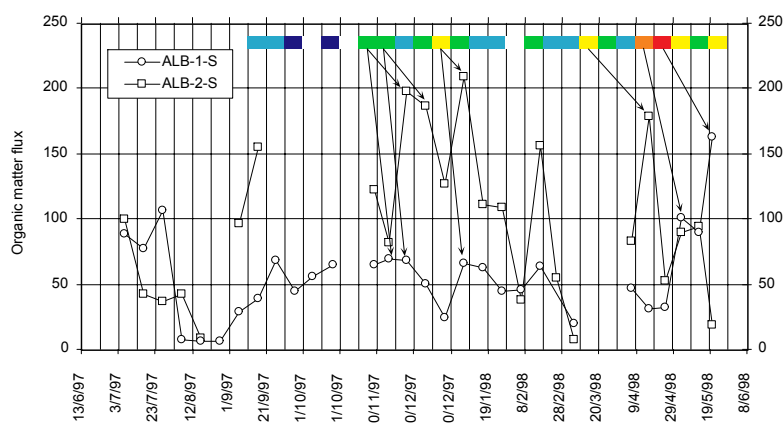


Figure 4.9. Temporal evolution of organic matter fluxes ($\text{mg}\cdot\text{m}^{-2}\cdot\text{d}^{-1}$) at mid water traps and chlorophyll-a concentrations ($\text{mg}\cdot\text{m}^{-3}$) in surface waters. The colour bar on the upper part of the graph is a summarised estimate of the chlorophyll-a concentrations derived from SeaWiFS images (Fig. 4.8, same colour code).

4.4.3.2. Temporal evolution of fluxes to near bottom waters

At some periods of the year total mass fluxes are higher in near-bottom waters than at mid waters (Fig. 4.10). These periods run from mid July to the end of August and from mid February to the end of May for the two stations. A third period with similar characteristics, from mid November to the end of December, concerns only the ALB-1 station. These increased fluxes to near-bottom traps are mainly due to the supply, in order of decreasing importance, of lithogenic, carbonate and opal material. As mentioned by Heussner et al. (1999) the depth increase of mass flux is a recurrent feature of particle transfer in continental slope environments that has been observed in most experiments performed so far. The exact processes involved may vary from one environment to another but scenarios proposed until now suggest that downslope transport is the principal mechanism that creates this increase by injecting and spreading supplementary amounts of settling particles at depth. And this is also quite probably the case in the WAB.

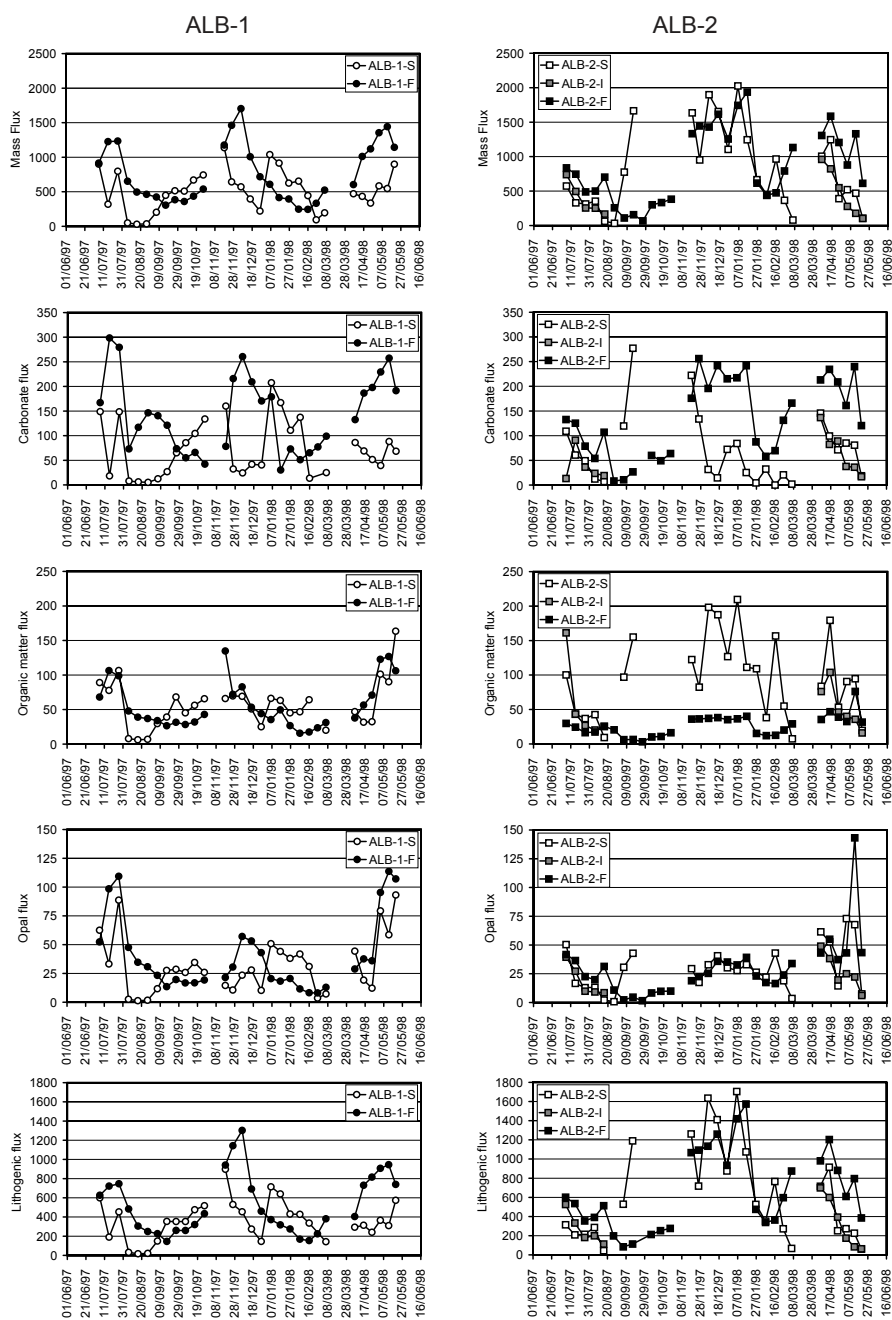


Figure 4.10. Temporal evolution of total mass fluxes and fluxes of main constituents ($\text{mg}\cdot\text{m}^{-2}\cdot\text{day}^{-1}$) at the two mooring stations.

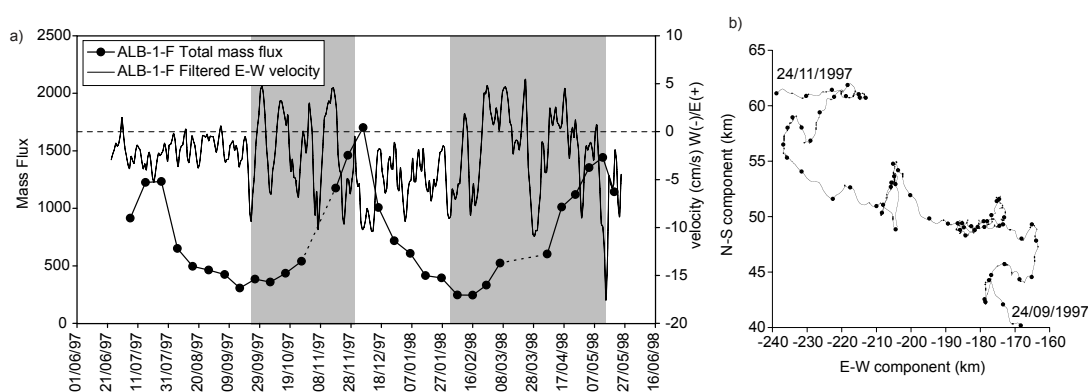


Figure 4.11. a) Temporal evolution of near-bottom particle fluxes (total mass in $\text{mg m}^{-2} \text{d}^{-1}$) and E-W low-pass filtered current component (cm s^{-1}). Shaded areas underline the 2 periods characterised by marked E-W current reversals resulting from an eddy-like activity. b) Progressive vector diagram of the near-bottom recorded current showing an eddy-like activity at ALB-1. The displayed period runs from 24/09/1997 to 24/11/1997. Dots represent days.

More interesting to notice is the fact that these periods of flux increase with depth result from well-marked flux events to the near-bottom ALB-1 trap. Each of these events culminates at maximum values around $1200\text{--}1700 \text{ mg m}^{-2} \text{d}^{-1}$, and is followed by a progressive decrease to a baseline value, around $300 \text{ mg m}^{-2} \text{d}^{-1}$ for the two periods observed in their entirety (Fig. 4.11a). We assume that the gaps between two consecutive deployments (2 weeks) do not substantially affect this temporal trend, and that fluxes during these periods would fit in the general, regular evolution of fluxes. If this assumption is correct, then the periods of flux increase last from June to mid-July 1997 (the exact start is not known since it took place before the beginning of the experiment) for the first one, from the end of September to the end of November 1997 for the second period, and from mid-February to mid-May 1998 for the third one. On Fig. 4.11a we also plot the low-pass filtered E-W current component that is responsible for most of the near-bottom current variability at ALB-1. The most striking feature that we observe is the periodic reversal of this component that results from an eddy-like activity (examples are given in Fig. 4.11b). This variability is well marked from the end of September to the end of November and from mid-February to the end of April, i.e. concomitantly to the periods of flux increase. Though we have no way to formally check the coupling between these parameters, the coincidence is striking enough to suggest a causal relationship between the dynamics of the water masses and the increase of mass fluxes. How the observed eddy-like structures influence the downward transfer of particles remains however beyond our knowledge and certainly deserves further study. Due to the lack of speed data for the near-bottom current meter in ALB-2 it is furthermore impossible to assess if the coincidence also holds for that station. The less regular temporal

evolution at this site suggests that the relationship could be less pronounced or more complex.

4.5. CONCLUSIONS

A number of conclusions regarding downward particle transfer and control mechanisms on the northern margin of the WAB may be drawn from this study.

(1) Measured downward particle fluxes in the WAB can be considered as reliable and present values (range of mean total mass fluxes of 503-855 $\text{mg}\cdot\text{m}^{-2}\cdot\text{d}^{-1}$) comparable to other slope sites. The particulate material collected by the traps is predominantly lithogenic (68-76%) and the wide range of temporal variation of total mass flux compared to the relative constancy in chemical composition determines that fluxes of major constituents essentially match those of total mass. A common temporal evolution can be observed in all traps, with a peak at the beginning of the summer, a broad composite peak during late autumn and winter and a third peak in spring.

(2) The main difference with regard to classical flux distributions in margin environments resides in the higher fluxes of organic matter to mid water depths at the offshore station (ALB-2). This unusual spatial feature could result from the funnelling or “subduction” of particles from the periphery of the surface WAG towards its centre. Surface and subsurface circulation appear therefore to exert an important control on particle transfer in this area of the Mediterranean Sea.

(3) The temporal evolution of the amount and composition of particle fluxes to mid waters is controlled by intermittent local fluvial discharge and oscillations in primary production on the periphery of the WAG. During late autumn and winter fluxes have a higher lithogenic content and temporal variability is mainly controlled by river sediment discharge. The arrival of nutrient-rich fresh waters to shelf areas could fertilise surface waters and trigger, together with other factors such as circulation-induced upwelling, the development of phytoplankton blooms that could feed synchronous biogenic particle sedimentation. In spring and summer fluxes are richer in organic matter and opal and their temporal variability is controlled by the development of phytoplankton blooms in surface waters. The lack of riverine inputs during this period of the year explains its lower contribution to total annual fluxes.

(4) There is a noticeable deep advective input of particles by mid-slope and basin bottom nepheloid layers stirred by near-bottom currents. Particles supplied by this mechanism are mainly of lithogenic and carbonate nature, with only a small organic contribution. Furthermore a temporal connection between near-bottom particle flux increase and eddy-like activity of water masses has been detected at least at one of the stations. The underlying mechanism remains unexplained.

Acknowledgements

J.F. would like to thank Nicole Delsaut from CEFREM for her lessons and assessment in trap preparation techniques. We also would like to thank Belen Oliva and Valentina Civano for their help during trap sample preparation. The Elemental Analysis, the ICP-AES and the Chemistry Laboratory teams of the “Serveis Científic Tècnics” of University of Barcelona provided invaluable help in carbon-nitrogen and silica analyses. We thank Francisco Plaza from University of Malaga for processing the CTD data. We are grateful to Frederic Melin from the Marine Environment Unit (ME) of the Space Applications Institute (SAI) for providing us with the SeaWiFS images and José María Díaz from the “Confederación Hidrográfica del Sur” for providing us with fluvial discharge data. We also want to thank Xavier Durrieu de Madron and two anonymous reviewers for their comments that helped us to improve the final manuscript. We are finally indebted with the officers, crew, technicians and scientists on board R/V Garcia del Cid and R/V Hespérides during the various MATER cruises for their help and dedication. J. F. was supported by an FPU grant (AP95 44002743) from “Ministerio de Educación y Ciencia”. The body of the research was supported by the EU MTPII-MATER project (MAS3-CT96-0051) to which the Spanish “Comisión Asesora de Investigación Científica y Técnica” and the Catalan “Comissió Interdepartamental per la Recerca i la Investigació Tecnològica” provided substantial co-funding. GRC Geociències Marines is additionally funded by “Generalitat de Catalunya” through its excellency research groups program (ref. 1999 SGR-63).

4.6. REFERENCES

- Antoine, D., Morel, A. and Andre, J.-M., 1995. Algal pigment distribution and primary production in the eastern Mediterranean as derived from coastal zone color scanner observations. *J. Geophys. Res.*, 100(C8): 16193-16209.
- Avila, A., Queralt-Mitjans, I. and Alarcon, M., 1997. Mineralogical composition of African dust delivered by red rains over Northeastern Spain. *J. Geophys. Res.*, 102(D18): 21977-21996.
- Baker, E.T., Milburn, H.B. and Tennant, D.A., 1988. Field assessment of sediment trap efficiency under varying flow conditions. *J. Mar. Res.*, 46: 573-592.
- Barcena, M.A. and Abrantes, F., 1998. Evidence of a high-productivity area off the coast of Malaga from studies of diatoms in surface sediments. *Mar. Micropal.*, 35: 91-103.
- Berman, S., 1990. Marine sediment reference materials for trace metals and other constituents. Marine Analytical Chemistry Standards Program, Division of Chemistry, National Research Council, Ottawa, Ontario, K1A0R6, 4 pp.
- British Oceanographic Data Centre, 1994. General bathymetric chart of the oceans (GEBCO): Birkenhead, Merseyside, England, Bidstone Obs. (CD-ROM).
- Buscail, R., Pocklington, R., Dumas, R. and Guidi, L., 1990. Fluxes and budget of organic matter in the benthic boundary layer over the Northwestern Mediterranean margin. *Cont. Shelf Res.*, 10(9-11): 1089-1122.
- Carratala, A., Bellot, J., Gomez, A., and Millan, M., 1996. African dust influence on rainwater on the eastern coast of Spain. In: S. Guerzoni and R. Chester (Editors), *The impact of desert dust across the Mediterranean*. Kluwer Academic Publishers, Amsterdam, pp. 323-332.
- Carter, T.G., Flanagan, J.P., Jones, C.R., Marchant, F.L., Murchinson, R.R., Rebman, J.H., Sylvester, J.C. and Whitney, J.C., 1972. A new bathymetric chart and physiography of the Mediterranean Sea. In: D.J. Stanley (Editor) *The Mediterranean Sea: A natural sedimentation laboratory*. Dowden, Hutchinson and Ross Inc., Stroudsburg, Pennsylvania, pp. 1-24.
- Cruzado, A., 1985. Chemistry of Mediterranean waters. In: R. Margalef (Editor), *Western Mediterranean*. Pergamon Press, Oxford, pp. 126-147.
- Dachs, J., Bayona, J.M., Fowler, S.W., Miquel, J.-C. and Albaiges, J., 1996. Vertical fluxes of polycyclic aromatic hydrocarbons and organochlorine compounds in the western Alboran Sea (Southwestern Mediterranean). *Mar. Chem.*, 52: 75-86.
- Dachs, J., Bayona, J.M., Fowler, S.W., Miquel, J.-C. and Albaiges, J., 1998. Evidence for cyanobacterial inputs and heterotrophic alteration of lipids in sinking particles in the Alboran Sea (SW Mediterranean). *Mar. Chem.*, 60: 189-201.

- Delgado, M., 1990. Phytoplankton distribution along the Spanish coast of the Alboran Sea. *Scient. Mar.*, 54(2): 169-178.
- Diaz, J.L. and Miranda, J.M., 1997. Tasas de deposición de polvo atmosférico en un área semiárida del entorno mediterráneo occidental. *Estudios Geol.*, 53: 211-220.
- Durrieu de Madron, X., Radakovitch, O., Heussner, S., Loye-Pilot, M. D. and Monaco, A., 1999. Role of climatological and current variability on shelf-slope exchanges of particulate matter: Evidence from the Rhône continental margin (NW Mediterranean). *Deep-Sea Res. I*, 46: 1513-1538.
- Earth Resources Information Systems Data Center, 1996. Global 30 seconds arc elevation dataset: Sioux Falls, South Dakota, U.S. Geological Survey (<http://edcwww.cr.usgs.gov/lansdaac/gtopo30/gtopo30.html>).
- Eisma, D., 1993. *Suspended matter in the aquatic environment*. Springer-Verlag. Berlin.
- Emelyanov, E.M. and Shimkus, K.H., 1986. *Geochemistry and sedimentology of the Mediterranean Sea*. Reidel Publishing Company, Dordrecht.
- Fabres, J., Calafat, A., Canals, M., Barcena, M.A. and Flores, J.A., 2000. Bransfield Basin fine-grained sediments: late-Holocene sedimentary processes and Antarctic oceanographic conditions. *The Holocene*, 10(6): 703-718.
- Fabres, J., Calafat, A., Sanchez-Vidal, A., Canals, M. and Heussner, S., (in prep). Particle fluxes during 1998 spring bloom in the Western Alboran Gyre: a high frequency flux experiment.
- Garcia-Gorriz, E. and Carr, M.-E., 1999. The climatological annual cycle of satellite-derived phytoplankton pigments in the Alboran Sea. *Geophys. Res. Lett.*, 26(19): 2985-2988.
- Gardner, W. D., 1985. The effect of tilt on sediment trap efficiency. *Deep-Sea Res.*, 32(3): 349-361.
- Gardner, W. D., Biscaye, P. E. and Richardson, M.J., 1997. A sediment trap experiment in the Vema Channel to evaluate the effect of horizontal particle fluxes on measured vertical fluxes. *J. Mar. Res.*, 55: 995-1028.
- Gomis, D., Ruiz, S. and Pedder, M. A., 2001. Diagnostic analysis of the 3D ageostrophic circulation from a multivariate spatial interpolation of CTD and ADCP data. *Deep-Sea Res.*, 48: 269-295.
- Guerzoni, S., Molinaroli, E. and Chester, R., 1997. Saharan dust inputs to the western Mediterranean Sea: depositional patterns, geochemistry and sedimentological implications. *Deep-Sea Res.*, 44(3-4): 631-654.
- Gust, G., Byrne, R.H., Bernstein, R.E., Betzer, P.R. and Bowles, W., 1992. Particle fluxes and moving fluids: experience from synchronous trap collections in the Sargasso Sea. *Deep-Sea Res.*, 39(7/8): 1071-1083.

- Gust, G., Michaels, A.F., Johnson, R., Deuser, W.G. and Bowles, W., 1994. Mooring line motions and sediment trap hydromechanics: in situ intercomparison of three common deployment designs. *Deep-Sea Res. I*, 41(5/6): 831-857.
- Heburn, G.W. and La Violette, P.E., 1990. Variations in the structure of the anticyclonic gyres found in the Alboran Sea. *J. Geophys. Res.*, 95(C2): 1599-1613.
- Heussner, S., Ratti, C. and Carbonne, J., 1990. The PPS 3 time-series sediment trap and the trap sample techniques used during the ECOMARGE experiment. *Cont. Shelf Res.*, 10(9-11): 943-958.
- Heussner, S., Calafat, A. and Palanques, A., 1996. Quantitative and qualitative features of particle fluxes in the North-Balearic Basin. In: M. Canals, J.L. Casamor, I. Cacho, A. Calafat, and Monaco, A (Eds) *Euromarge-NB Final Report, MAST II Programme, EU, Vol. II, chapter. n. 3, pp. 41-66.*
- Heussner, S., Durrieu de Madron, X., Radakovitch, O., Beaufort, L., Biscaye, P.E., Carbonne, J., Delsaut, N., Etcheber, H. and Monaco, A., 1999. Spatial and temporal patterns of downward particle fluxes on the continental slope of the Bay of Biscay (Northeastern Atlantic). *Deep-Sea Res. II*, 46: 2101-2146.
- Huang, T-C and Stanley, D. J., 1972. Western Alboran Sea: Sediment dispersal, ponding and reversal of currents. In: D. J. Stanley (Editor), *The Mediterranean Sea: A natural sedimentation laboratory.* Dowden, Hutchison and Ross, Inc., Stroudsburg, Pennsylvania, pp. 521-559.
- Kamatani, A. and Oku, O., 2000. Measuring biogenic silica in marine sediments. *Mar. Chem.*, 68: 219-229.
- Kinder, T.H. and Parrilla, G., 1987. Yes, Some of the Mediterranean Outflow Does Come From Great Depth. *J. Geophys. Res.*, 92(C3): 2901-2906.
- La Violette, P. E., 1984. The advection of submesoscale thermal features in the Alboran Sea Gyre. *J. Geophys. Res.*, 14: 550-565.
- La Violette, P. E., 1995. Overview of the major forcings and water masses of the Western Mediterranean Sea. In: P. E. La Violette (Editor), *Seasonal and interannual variability of the western Mediterranean Sea (Coastal and Estuarine Studies, 46).* American Geophysical Union, Washington DC, pp. 1-11.
- Martin, J.H., Knauer, J.A., Karl, D.M. and Broenkow, W.W., 1987. VERTEX: carbon cycling in the Northeast Pacific. *Deep-Sea Res.*, 34: 267-285.
- Martins, O. and Probst, J-L., 1991. Biogeochemistry of major African rivers: Carbon and mineral transport. In: E. T. Degens, S. Kempe and J.E. Richey (Editors), *Biogeochemistry of Major World Rivers.* SCOPE Report 42. John Wiley and Sons Ltd., Chichester, pp. 127-155.

- Melin, F., 2000. SeaWiFS images archive, SeaWiFS dataset for the Eastern Atlantic. September 1997- May 1998. Space Applications Institute (SAI), Marine Environment Unit (ME), Joint Research Centre (JRC), online dataset http://me-www.jrc.it/me-website/contents/shared_utilities/frames/archive_seawifs.htm.
- Melin, F., Bulgarelli, B., Gobron, N., Pinty, B., and Tacchi, R., 2000. An integrated tool for SeaWiFS operational processing. Joint Research Centre Publication, No. EUR 19576 EN. Space Applications Institute (SAI), Marine Environment Unit (ME), Joint Research Centre (JRC).
- Millot, C., 1987. Circulation in the Western Mediterranean Sea. *Oceanol. Acta*, 10(2): 143-149.
- Minas, H.J., Coste, B., Le Corre, P., Minas, M. and Raimbault, P., 1991. Biological and Geochemical Signatures Associated With the Water Circulation Through the Strait of Gibraltar and in the Western Alboran Sea. *J. Geophys. Res.*, 96(C5): 8755-8771.
- Miquel, J.C., Fowler, S.W., La Rosa, J. and Buat-Menard, P., 1994. Dynamics of the downward flux of particles and carbon in the open northwestern Mediterranean Sea. *Deep-Sea Res. I*, 41(2): 243-261.
- Miserochchi, S., Faganeli, J., Balboni, V., Heussner, S., Monaco, A. and Kerherve, P., 1999. Characteristics and sources of the settling particulate organic matter in the South Adriatic Basin. *Org. Geoch.*, 30: 411-421.
- Monaco, A., Biscaye, P., Soyer, J., Pocklington, R. and Heussner, S., 1990. Particle fluxes and ecosystem response on a continental margin: the 1985-1988 Mediterranean ECOMARGE experiment. *Cont. Shelf Res.* 10(9-11): 809-839.
- Monaco, A., Durrieu de Madron, X., Radakovitch, O., Heussner, S. and Carbonne, J., 1999. Origin and variability of downward biogeochemical fluxes on the Rhone continental margin (NW Mediterranean). *Deep-Sea Res. I*, 46: 1483-1511.
- Morel, A. and Andre, J.-M., 1991. Pigment distribution and primary production in the Western Mediterranean as derived and modelled from Coastal Zone Color Scanner observations. *J. Geophys. Res.*, 96(C7): 12685-12698.
- Mortlock, R.A. and Froelich, P.N., 1989. A simple method for the rapid determinations of biogenic opal in pelagic marine sediments. *Deep-Sea Res.*, 36(9): 1415-1426.
- Nieuwenhuize, J., Maas, Y.E.M. and Middelburg, J.J., 1994. Rapid analysis of organic carbon and nitrogen in particulate materials. *Mar. Chem.*, 45: 217-224.
- Packard, T.T., Minas, H.J., Coste, B., Martinez, R., Bonn, M.C., Gostan, J., Garfield, P., Christensen, J., Dortch, Q., Minas, M., Copin-Montegut, G. And Copin-Montegut, C.,

1988. Formation of the Alboran oxygen minimum zone. *Deep-Sea Res.* 35(7): 1111-1118.
- Palanques, A. and Biscaye, P. E., 1992. Patterns and controls of the suspended matter distribution over the shelf and upper slope south of New England. *Cont. Shelf Res.*, 12(5/6): 577-600.
- Parrilla, G., Kinder, T.H. and Preller, R.H., 1986. Deep and Intermediate Mediterranean Water in the western Alboran Sea. *Deep-Sea Res.*, 33(1): 55-88.
- Peinert, R.D., Fowler, S.W., Hamilton, T.F., La Rosa, J. and Barlow, R.G., 1993. Vertical particulate fluxes in relation to suspended particles in the western Alboran Sea. In: J.-M. Martin and H. Barth (Editors), *Proceedings of the 4th Eros 2000 (European River Ocean System) workshop 28 Sept.- 2 Oct. 1992, Plymouth, UK.* *Water Poll. Res. Rep.*, 30: 195-201.
- Peinert, R. and Miquel, J.-C., 1994. The significance of frontal processes for vertical particle fluxes: A case study in the Alboran Sea (SW Mediterranean Sea). *J. Mar. Syst.*, 5: 377-389.
- Pistek, P., De Strobel, F. and Montanari, C., 1985. Deep-sea circulation in the Alboran Sea. *J. Geophys. Res.*, 90(C3): 4969-4976.
- Plaza, F., 2001. Variabilidad temporal en la Cuenca Occidental del Mar de Alborán y su relación con los flujos a través del Estrecho de Gibraltar y Pasaje de Alborán. Ph.D. Thesis. Univ. Cádiz, Spain, unpublished.
- Puig, P. and Palanques, A., 1998a. Temporal variability and composition of settling particulate fluxes on the Barcelona continental margin. *J. Mar. Res.*, 56, 639-654.
- Puig, P. and Palanques, A., 1998b. Nepheloid structure and hydrographic control on the Barcelona continental margin, eastern Spain. *Mar. Geol.* 149 (1-4): 39-54.
- Roda, F., Bellot, J., Avila, A., Escarre, A., Pinol, J. and Terradas, J., 1993. Saharan dust and the atmospheric inputs of elements and alkalinity to Mediterranean ecosystems. *Water, Air and Soil Pollution*, 66: 277-288.
- Ruiz, J., Echevarria, F., Font, J., Ruiz, S., García, E., Blanco, J. M., Jiménez-Gómez, F., Prieto, L., González-Alaminos, A., García, C. M., Cipollini, P., Snaith, H., Bartual, A., Reul, A., Rodríguez, V., 2001. Surface distribution of chlorophyll, particles and gelbstoff in the Atlantic jet of the Alboran Sea: from submesoscale to subinertial scales of variability. *J. Mar. Sys.*, 29: 277-292.
- Salisbury, J. E., Campbell, J. W., Meeker, L. D. and Vörösmarty, C., 2001. Ocean color and river data reveal influence in coastal waters. *EOS*, 82 (20): 221- 227.
- Sarhan, T., García-Lafuente, J., Vargas, M., Vargas, J. M. and Plaza, F., 2000. Upwelling mechanisms in the Northwestern Alboran Sea. *J. Mar. Sys.*, 23: 317-331.

- Siegel, D.A. and Deuser, W.G., 1997. Trajectories of sinking particles in the Sargasso Sea: modeling of statistical funnels above deep-ocean sediment traps. *Deep-Sea Res. I*, 44(9-10): 1519-1541.
- Sparnocchia, S., Manzella, G.M.R., and La Violette P.E., 1995. The interannual and seasonal variability of the MAW and LIW core properties in the Western Mediterranean Sea. In: P. E. La Violette (Editor), *Seasonal and interannual variability of the western Mediterranean Sea (Coastal and Estuarine Studies; 46)*. American Geophysical Union, Washington DC, pp. 177-194.
- Tintore, J., La Violette, P.E., Blade, I. and Cruzado, A., 1988. A Study of an Intense Density Front in the Eastern Alboran Sea: The Almeria-Oran Front. *J. Phys. Oceanogr.*, 18: 1384-1397.
- Tomadin, L., Lenaz, R., Landuzzi, V., Mazzucotelli, A. and Vannucci, R., 1984. Wind-blown dusts over the Central Mediterranean. *Oceanol. Acta*, 7(1): 13-23.
- Viudez, A., Pinot, J.-M. and Haney, R.L., 1998. On the upper layer circulation in the Alboran Sea. *J. Geophys. Res.*, 103(C10): 21653-21666.

